Theoretical Study of Extinction Ratio and Frequency Chirping of VCSEL-Based Two-Dimensional Wavelength Converter

H. Liu, P. Shum, *Member, IEEE*, and M. S. Kao, *Member, IEEE*

***Abstract*—A novel two-dimensional (2-D) vertical-cavity surface-emission laser (VCSEL)-based wavelength converter was reported, in which the VCSEL was used both as the laser source for the probe wave and as the semiconductor amplifier for performing cross-gain modulation. We have developed a complete 2-D transmission line laser model to analyze the proposed structure. The optimization of the wavelength location, input power level, as well as the reflectivity of the VCSEL facet have been done with respect to the extinction ratio and peak chirp frequency.**

***Index Terms*—Extinction ratio (ER), transmission line laser modeling, vertical-cavity surface-emitting lasers (VCSELs), wavelength converters.**

I. Introduction

ALL-OPTICAL wavelength converters are expected to become key components in future broad-band networks. Several techniques had been proposed to achieve wavelength conversion. One simple technique for transferring information from one wavelength to another is the use of the cross-gain modulation (XGM) in semiconductor amplifiers (SOAs) [1]. The input signal can be launched either copropagation or counterpropagation into the SOA. However, shortcomings exist in these two configurations. For the copropagating injection, an optical filter is needed to suppress the signal wave. For the counterpropagating method, though optical filter is avoided, additional isolator at the probe input is required to suppress the strongly amplified input signal [2]. The problem of isolation can be resolved by launching the input signal and the converted probe wavelength at orthogonal directions. 2-D side-injection light-controlled bistable laser diodes had been reported by Nonaka *et al.* [3]. The results revealed that SOA-based 2-D devices were quite promising for optical signal processing.

Recently, we proposed a novel 2-D vertical-cavity surface-emission laser (VCSEL)-based wavelength converter [4]. In this configuration, the VCSEL acts as the laser source for the probe wave and as the SOA to perform XGM effect. The probe wave and the signal wave will propagate along orthogonal directions with the advantage of simplifying the structure. We develop a modified transmission line laser model (TLLM) to describe the VCSEL-based wavelength converter. The dynamic characteristics of the proposed wavelength converter are of interest, and here we apply the TLLM to further investigate extinction ratio (ER), frequency chirping, and optical pulse patterns of this device by taking account of the wavelength region of both signal wave and probe wave, the input power of the signal wave and the reflectivity of the facets.

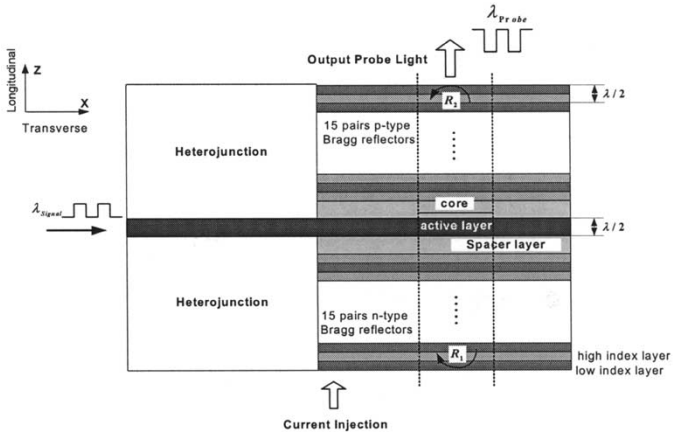

Fig. 1. VCSEL-based 2-D wavelength converter.

II. 2-D TLLM for VCSEL-Based Wavelength Converter

The VCSEL-based wavelength converter is shown in Fig. 1. Here, we adopted the VCSEL structure [5] and extended the active region at the horizontal direction. In this structure, the extended active region was used to amplify the input signal wave, which guarantees a strong XGM effect. By this means, high ER of the probe wave can be achieved. By employing this structure, two main advantages will be provided. First, additional devices such as optical filter or optical isolator are not required anymore. Second, additional laser source for the probe wave can be saved because the VCSEL works as a laser source as well as an amplifier.

To analyze the characteristics of the proposed structure, a 2-D TLLM is required. Details of one-dimensional (1-D) TLLM had been given in [6], and Nguyen *et al.* [7] have developed a 1-D model supporting two orthogonal polarizations. We have developed a 2-D TLLM model for the proposed structure [4]. In the developed model, the forward and the backward probe waves are named F_P and B_P, and those of the signal wave are named

Manuscript received July 7, 2003; revised September 11, 2003.

H. Liu and P. Shum are with the Network Technology Research Center, Nanyang Technological University, Singapore 639798, Singapore (e-mail: pg00839373@ntu.edu.sg).

M. S. Kao is with the Department of Communication Engineering, National Chiao-Tung University, Hsinchu 30050, Taiwan, R.O.C.

Digital Object Identifier 10.1109/LPT.2003.821238

1041-1135/04$20.00 © 2004 IEEE

F_S and B_S, respectively. We describe the scattering process at time t of these four waves in the active region as

$$ {}_t[F_{S,P}(n,m)]^r = S_{S,P} * {}_t[F_{S,P}(n,m)]^i + {}_t\left[I_{\rm sp}(n,m)Z_p\frac{T}{2}\right] \quad (1)$$

$$ {}_t[B_{S,P}(n,m)]^r = S_{S,P} * {}_t[B_{S,P}(n,m)]^i + {}_t\left[I_{\rm sp}(n,m)Z_p\frac{T}{2}\right] \quad (2)$$

where i denotes the incident wave, r denotes the reflected wave, S_S is the scattering matrix for the signal wave, S_P is the scattering matrix for the probe wave, $I_{\rm sp}$ is the spontaneous noise current, Z_p is the cavity wave impedance, T is the attenuation, and n and m are the section numbers in the traveling direction of the probe wave and the signal wave, respectively. The amplified spontaneous emission (ASE) noise is modeled with noise current $I_{\rm sp}$, which is represented by three statistically independent Gaussian distributed random processes [6], [8].

The connecting process which connects two scattering nodes together can be written as [5]

$$ {}_{t+1}\begin{bmatrix} F_{S,P}(n+1,m) \\ B_{S,P}(n,m) \end{bmatrix}^i = C_{S,P} * {}_t\begin{bmatrix} F_{S,P}(n,m) \\ B_{S,P}(n+1,m) \end{bmatrix}^r \quad (3)$$

where C_P is the connecting matrix for the probe wave and C_S is the connecting matrix for the signal wave. It should be noted that C_P and C_S are identity matrices for those sections where there are no distributed Bragg reflectors (DBRs).

However, out of the XGM area, DBR exists in the vertical direction. In these sections, C_P is not identity matrix anymore and should be modified to reflect the wave coupling and reflection in DBR. To represent wave changes at the Bragg reflectors, we employ the connecting matrices using the effective index method [6]

$$C_P = \begin{bmatrix} \frac{2\sqrt{n_l n_h}}{(n_l+n_h)} & \frac{-(n_l-n_h)}{(n_l+n_h)} \\ \frac{(n_l-n_h)}{(n_l+n_h)} & \frac{2\sqrt{n_l n_h}}{(n_l+n_h)} \end{bmatrix}. \quad (4)$$

Here n_l is the effective index of the low index layer and n_h is the effective index of the high index layer. The chirp of the converted signals is calculated by differentiating its phase with respect to time $[-1/(2\pi)(d\phi/dt)]$.

III. Results and Discussion

The proposed structure has been analyzed by applying the improved TLLM. The simulation parameters were shown in [4]. Fig. 2 shows the pulse patterns of probe wave (upper) and signal wave (middle) as well as peak chirp frequency (lower) at the bit rate of 2.5 Gb/s. In the simulation, the signal wave is located at the gain peak and the probe wavelength was at -40-nm shift from the gain peak. Moreover, the input signal power refers to the power after amplification. The frequency chirping due to dynamic change of the carrier density was observed in Fig. 2. It was found that negative peak chirp frequency is larger than the positive one since the fall time is shorter than the rise time. Fig. 2 also shows that ASE noise is smaller at the low state than at the high state, since gain saturation may reduce the ASE noise at high input signal power.

Fig. 3 shows the contour plot of the output ER for the signal wavelength and the probe wavelength in the region of $1515 \sim 1615$ nm. Owing to the asymmetric gain profile, we observe that down-conversion ($\lambda_{\rm Probe}$ is shorter than $\lambda_{\rm Signal}$) leads to a higher ER than that of up-conversion ($\lambda_{\rm Probe}$ is longer than $\lambda_{\rm Signal}$). The peak chirp contour map with respect to the signal and the probe wavelengths can also be calculated. We observe that at the wavelength where high ER is obtained, large peak chirp frequencies also appear due to shorter rise time and fall time of the converted wave. Therefore, the optimum wavelength region of signal wave and probe wave can be found by considering both of the ER and peak chirp frequency. In Fig. 3, the shadow region indicates the optimum wavelength region, where ER is higher than 10 dB, and peak chirp frequency is between -3.5 and 3 GHz.

The evolution of ER and peak chirp of the probe wave in the transverse direction at different facet reflectivity is shown in Fig. 4. We observe that ER increases along the transverse direction because of the amplification of the signal power in this direction, and the lower the reflectivity, the higher ER is obtained due to the stronger amplification effect. On the other hand, the peak chirp is also affected by the reflectivity. With high reflectivity, the amplification of the signal wave will be reduced as more carriers are consumed by the probe wave. Therefore,

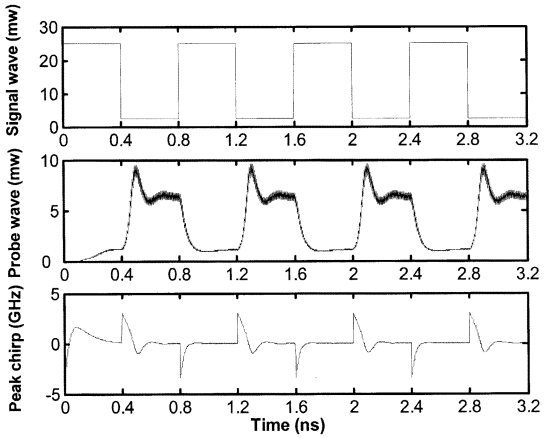

Fig. 2. Pulse pattern of probe wave (upper), signal wave (middle), and peak chirp frequency (lower) at 2.5 Gb/s ($R_1 = 97.4\%$, $R_2 = 55\%$, $\lambda_{\rm Signal} = 1565$ nm, and $\lambda_{\rm probe} = 1525$ nm. ER of input signal $= 10$ dB. Input power $= 25$ mw).

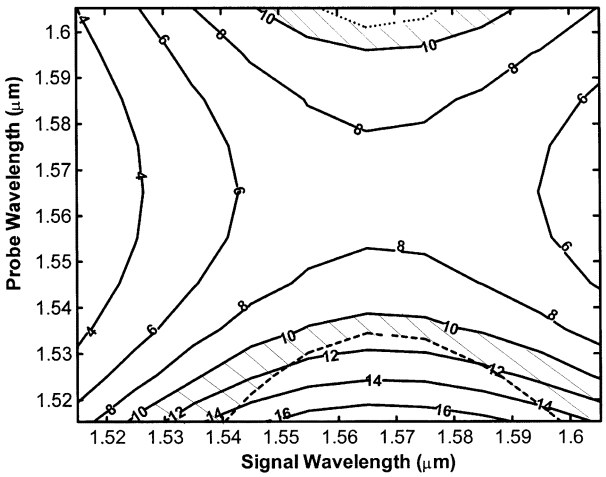

Fig. 3. Contour plot of the ER with respect to signal wavelength and probe wavelength ($R_1 = 97.4\%$ and $R_2 = 55\%$. ER of input signal $= 10$ dB. Input power $= 25$ mw).

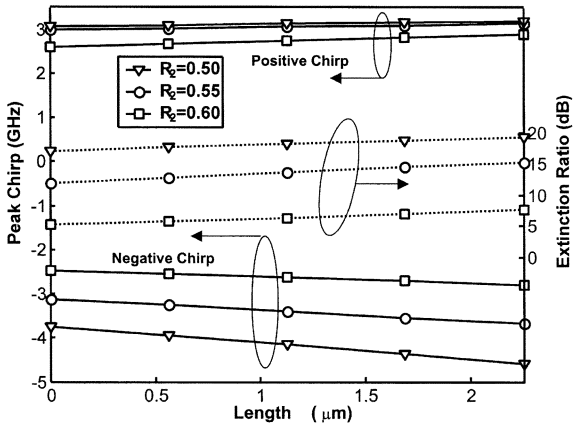

Fig. 4. Evolution of peak chirp frequency and ER in the transverse direction of the probe wave at different facet reflectivity. ($R_1 = 97.4\%$.)

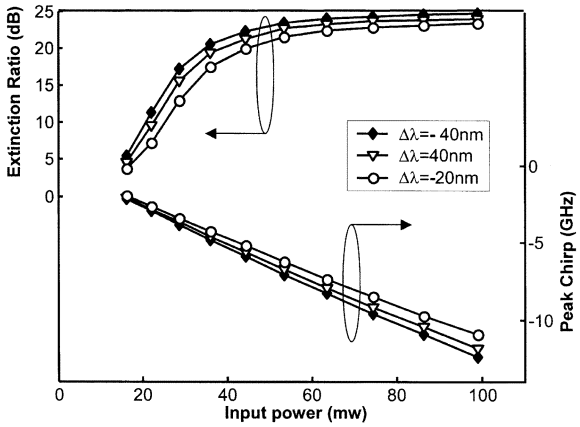

Fig. 5. Negative peak chirp frequency and ER of the probe wave as a function of input signal power at with different wavelength locations ($R_1 = 97.4\%$, $R_2 = 55\%$. $\lambda_{\text{Signal}} = 1565$ dB).

the XGM will be weakened which results in longer rise time and fall time for the probe wave. Fig. 4 reveals that high reflectivity leads to a lower peak chirp frequency because of the longer rise time and fall time.

We have investigated the effects of input power on the ER and chirping in Fig. 5. In the calculation, wavelength difference of signal wave and probe wave $\Delta\lambda$ equal to -40, -20, and 40 nm, respectively, is analyzed where signal wavelength is fixed at the peak of the gain spectrum. In the simulation, the input ER is kept at 10 dB as the power of input signal varies. From the results, we see that the ER and the negative peak chirp frequency increase with the input power, however, the ER saturates when the input power is above 80 mw. The observed ER saturation can be explained as follows. The ER of the probe wave depends on the "1" state level of the signal wave. As "1" state of input signal increases to a specified level, it will consume almost all the carriers and make the probe wave work under lasing threshold. After this critical point, even the input power increased, the "0" state of the probe wave will keep at a constant. On the other hand, the "0" state of the input signal has little effect on the XGM. Therefore, the output of the probe wave will mainly depend on the "1" state of the probe wave.

The effects of facet reflectivity on the ER and peak chirp have also been analyzed. In our analysis, R_1 is fixed at 97.4% and R_2 varies from $45\% \sim 65\%$ with different input powers. Fig. 6

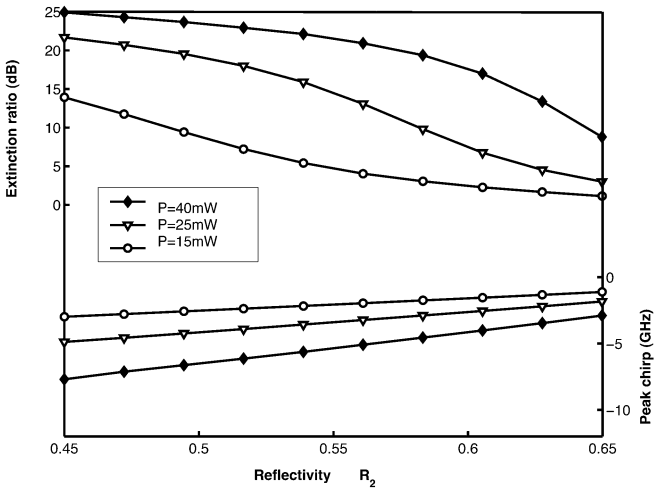

Fig. 6. Negative peak chirp frequency and ER of the probe wave as a function of facet reflectivity for different input powers. ($R_1 = 97.4\%$.)

shows that the ER decreased while the reflectivity R_2 increased. This is because more carriers are consumed for high reflectivity, thereby leading to weakened XGM effect. Moreover, when the input power is high, strong XGM effect will be produced. As expected, high ER is observed in Fig. 6 at high input power.

IV. Conclusion

We have reported on a complete dynamic TLLM model for a novel 2-D VCSEL-based wavelength converter. The proposed VCSEL is used both as the laser source for the probe wave and as an SOA for performing XGM. In our investigation, the optimization of the wavelength location, input power level, as well as the reflectivity of the VCSEL facet have been analyzed with respect to the ER and peak chirp frequency. We show that a wide-band wavelength converter can be designed by employing the proposed 2-D structure.

References

[1] T. Durhuus, B. Mikkesen, C. Joergensen, S. L. Danieselen, and K. E. Stubjkaer, "All-optical wavelength conversion by semiconductor optical amplifiers," *J. Lightwave Technol.*, vol. 14, pp. 943–954, June 1996.

[2] K. Obermann, S. Kindt, D. Breuer, and K. Petermann, "Performance analysis of wavelength converters based on cross-gain modulation in semiconductor-optical amplifiers," *J. Lightwave Technol.*, vol. 16, pp. 78–85, Jan. 1998.

[3] K. Nonaka, F. Kobayashi, K. Kishi, T. Tadokoro, Y. Itoh, C. Amano, and T. Kurokawa, "Direct time domain optical demultiplexing of 10-Gb/s NRZ signals using side-injection light-controlled bistable laser diode," *IEEE Photon. Technol. Lett.*, vol. 10, pp. 1484–1486, Oct. 1998.

[4] H. Liu, P. Shum, and M. S. Kao, "Design and analysis of VCSEL based two dimension wavelength converter," *Opt. Express*, vol. 14, pp. 1659–1668, 2003.

[5] S. F. Yu, "An improved time-domain travelling-wave model for vertical-cavity surface-emitting lasers," *IEEE J. Quantum Electron.*, vol. 34, pp. 1938–1948, Oct. 1998.

[6] A. J. Lowery, "Transmission-line modeling of semiconductor lases: The transmission-line laser model," *Int. J. Numer. Modeling: Electronic Networks, Devices and Fields*, vol. 2, pp. 249–265, 1989.

[7] L. V. T. Nguyen, A. J. Lowery, and D. Novak, "Large- and small-signal dynamic behavior of high-speed dual-polarization quantum-well semiconductor lasers," *IEEE J. Select. Topics Quantum Electron.*, vol. 3, pp. 279–289, Apr. 1997.

[8] H. Lee, H. Yoon, Y. Kim, and J. Jeong, "Theoretical study of frequency chirping and extinction ratio of wavelength-converted optical signals by XGM and XPM using SOAs," *IEEE J. Quantum Electron.*, vol. 35, pp. 1213–1219, Aug. 1999.